Acta Oceanol. Sin., 2022, Vol. 41, No. 1, P. 39–49
https://doi.org/10.1007/s13131-021-1978-9
http://www.aosocean.com
E-mail: ocean2@hyxb.org.cn

Oceanic crustal structure and tectonic origin of the southern Kyushu-Palau Ridge in the Philippine Sea

Xiongwei Niu[1, 3], Pingchuan Tan[1, 3*], Weiwei Ding[1, 2, 3*], Wei Wang[1, 2], Yao Wei[1], Xiaodong Wei[1, 3], Aiguo Ruan[1, 2, 3], Jie Zhang[1, 3], Chunyang Wang[1, 3], Yong Tang[1, 2, 3], Jiabiao Li[1, 2]

[1] Key Laboratory of Submarine Geosciences, Ministry of Natural Resources/Second Institute of Oceanography, Ministry of Natural Resources, Hangzhou 310012, China

[2] School of Oceanography, Shanghai Jiao Tong University, Shanghai 200240, China

[3] Southern Marine Science and Engineering Guangdong Laboratory (Zhuhai), Zhuhai 519080, China

Received 1 December 2021; accepted 15 December 2021

Abstract

A new high-resolution velocity model of the southern Kyushu-Palau Ridge (KPR) was derived from an active-source wide-angle seismic reflection/refraction profile. The result shows that the KPR crust can be divided into the upper crust with the P-wave velocity less than 6.1 m/s, and lower crust with P-wave velocity between 6.1 km/s and 7.2 km/s. The crustal thickness of the KPR reaches 12.0 km in the center, which gradually decreases to 5.0–6.0 km at sides. The velocity structure of the KPR is similar to the structures of the adjacent West Philippine Basin and Parece Vela Basin (PVB), indicating a typical oceanic crust. Isostatic analysis shows that some regional compensation occurs during the loading of the KPR, which implies that the KPR was built mainly by magmatism during the splitting of the Izu-Bonin-Mariana arc and the following back-arc seafloor spreading of the PVB during 30–28 Ma BP. The absence of the thick middle crust (6.0–6.5 km/s) and high velocity lower-crustal layers (7.2–7.6 km/s) suggest that arc magmatism plays a less important role in the KPR formation.

Key words: P-wave crustal structure, ocean bottom seismometer, Kyushu-Palau Ridge, oceanic crust

Citation: Niu Xiongwei, Tan Pingchuan, Ding Weiwei, Wang Wei, Wei Yao, Wei Xiaodong, Ruan Aiguo, Zhang Jie, Wang Chunyang, Tang Yong, Li Jiabiao. 2022. Oceanic crustal structure and tectonic origin of the southern Kyushu-Palau Ridge in the Philippine Sea. Acta Oceanologica Sinica, 41(1): 39–49, doi: 10.1007/s13131-021-1978-9

1 Introduction

The Izu-Bonin-Marina arc (IBM) subduction system is a typical representative of the large-scale convergence boundary in the world, having strong lithospheric deformation and magmatic activity in the West Pacific. It forms a typical "trench-arc-basin" system with an eastward transition of the back-arc spreading due to the westward subducting Pacific Plate (Fig. 1). It is widely considered as an ideal area to study the "subduction factory" as well as the seismic activities of the subduction zone (Ishizuka et al., 2011a, b). In the western part, the IBM subduction system has a remnant arc, namely the Kyushu-Palau Ridge (KPR); whereas the modern IBM volcanic island arc belt (such as the Izu-Ogasawara Ridges and Mali Yana Island Arc) lies in the east. Several Cenozoic oceanic basins developed in-between, including the Shikoku Basin, Parece Vela Basin (PVB), Ogasawara Trough, and Mariana Trough (Fig. 1).

The KPR extends from the Nankai Trough in the north to the northern part of the Palau Archipelago in the south. It is a bathymetric high extending through the Philippine Sea Plate with a total length of 2 600 km (Fig. 1). It was once connected with the modern IBM island arc belt before the splitting of the proto-IBM arc and the back-arc spreading with the continuous retreat of the Pacific Plate subduction at about 30 Ma BP (Stern et al., 2004). Therefore, the KPR should be firstly built by the initial subduction between the proto-Pacific Plate under the West Philippine Basin (WPB), and then modified by the magmatic activity after the breakup of the proto-IBM island arc. However, how magmatism controlled the growth of the KPR is still debatable.

Seismic velocity models can be used to provide a crisis information for the mechanisms of the growth of the island arc crust. The previous deep reflection/refraction seismic explorations carried out on the KPR were completed mainly by Japanese scientists (Murauchi et al., 1968; Arisaka et al., 2003; Nishizawa et al., 2007, 2016). Especially during 2004–2008, the Japan Agency for Marine-Earth Science and Technology conducted a series of seismic experiments on the KPR and presented 27 wide-angle seismic profiles to understand its lithospheric structural changes from north (31°N) to south (13°N) (Nishizawa et al., 2016). Their results showed that the KPR has a large variation in crustal thickness (8–23 km), which is generally larger than those oceanic crust of the surrounding back-arc basin, such as the PVB in the east and the WPB in the west. The growth of the thick crust is accommodated mainly by accretion of the lower crust (6.8–7.0 km/s), whereas for crustal thickness greater than 20 km, it also has a rel-

Foundation item: The National Natural Science Foundation of China under contract Nos 91858214 and 41890811; the Scientific Research Fund of the Second Institute of Oceanography, MNR under contract No. HYGG2001; the National Natural Science Foundation of China under contract Nos 42006072, 41876060, 41776053 and 42076080; the National Program on Global Change and Air-Sea Interaction, MNR under contact No. GASI-02-PAC-DWZP02; the Innovation Group Project of Southern Marine Science and Engineering Guangdong Laboratory (Zhuhai) under contract No. 311020018.
*Corresponding author, E-mail: tanpc@sio.org.cn; wwding@sio.org.cn

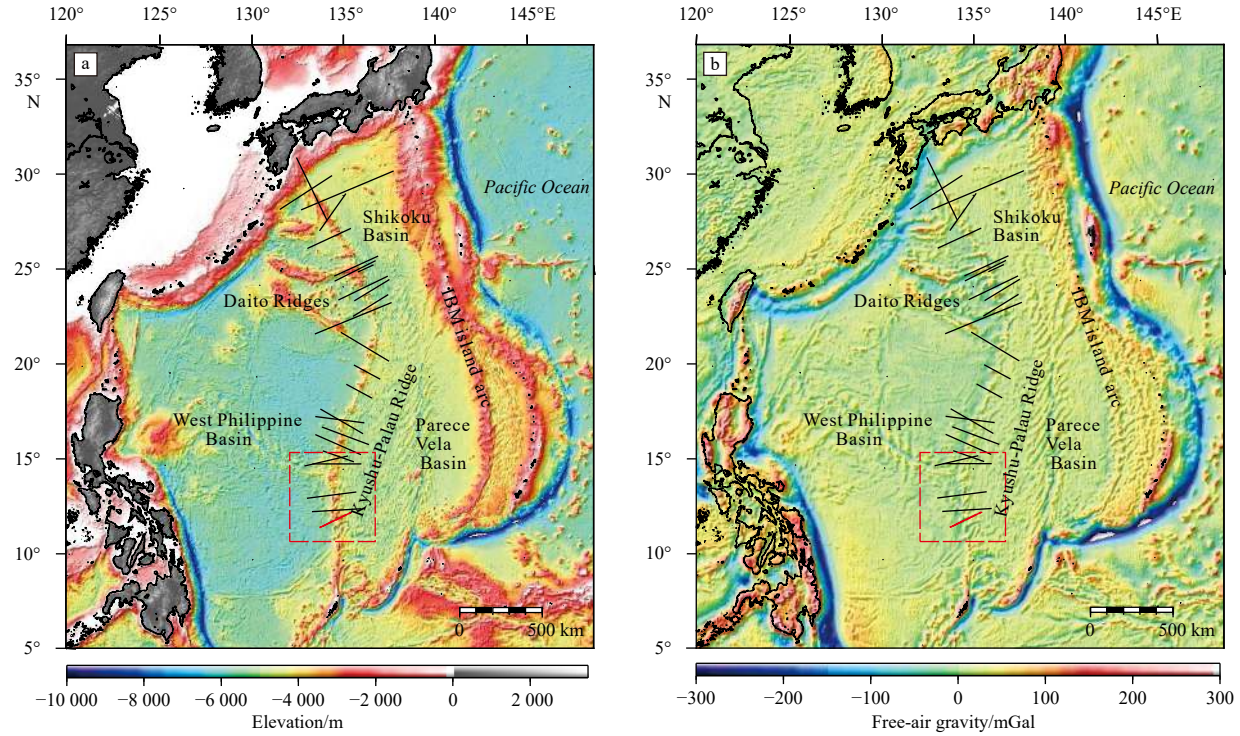

Fig. 1. Bathymetry (a, Tozer et al., 2019) and free air gravity (1 Gal=1 cm/s²) (b, Sandwell et al., 2014) of the Mariana arc-back-arc region with locations of the wide-angle seismic refraction profiles, where the study area is indicated by a red dashed rectangle. The black solid lines show the profiles from Nishizawa et al. (2016), while the red solid line shows the profile of this study.

atively thick (>5 km) middle crust with a P-wave velocity (V_p) of ~6 km/s. Some high velocity lower-crust layers are also observed under the KPR with a relatively high V_p of 7.2 km/s (Nishizawa et al., 2016). Two wide-angle seismic profiles cross the southern part of the KPR (south of 15°N) (Figs 1 and 2), but show a different crustal structure (Nishizawa et al., 2016). One profile (ID: Kpr40, near 14°N) indicate that the KPR crust has a crustal "root" with an average lower crustal velocity of 7.2 km/s. The crust is 15 km thick, and its thickening is attributed mainly to the accretion of the middle and lower crust. The other profile crossing the KPR ridge (ID: Kpr41, near 13 °N) lacks the high velocity at lower crustal layer and crustal "root" with a very thin (<2 km) middle crustal layer. The crustal thickness is 10 km (Nishizawa et al., 2016).

According to the above, seismic experiments focused mainly on the northern part of the KPR (north of 15°N) (Fig. 1), and the crustal structure of the southern part (south of 15°N) has limited data and is less understood. To better understand the crustal

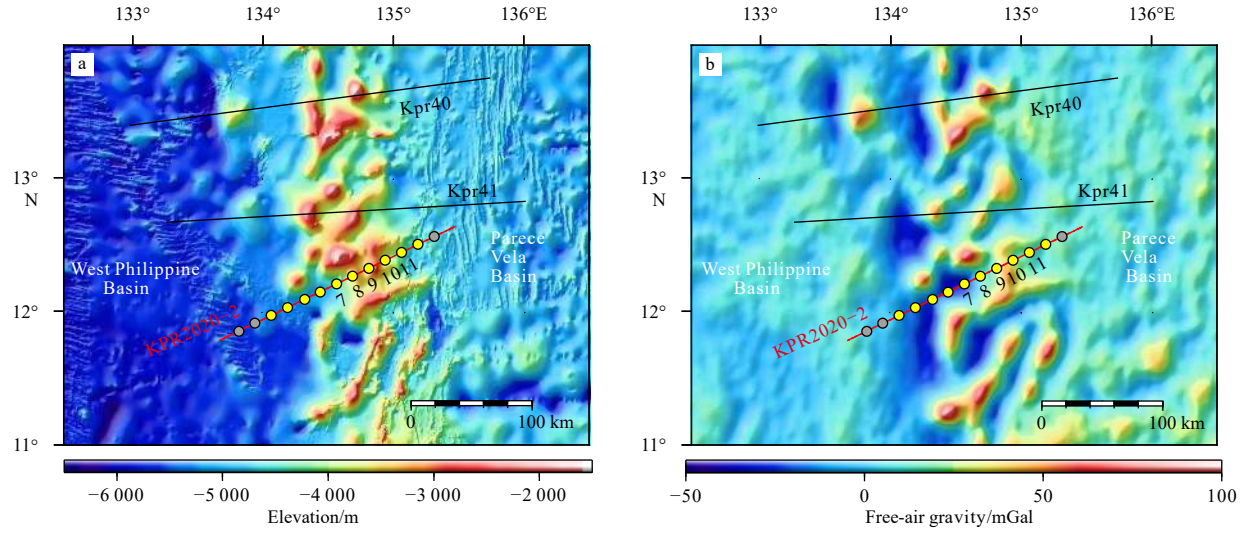

Fig. 2. Seismic refraction profiles shown on bathymetry (a) and free-air gravity (1 Gal=1 cm/s²) (b) of the southern part of the KPR. The red line is the ocean bottom seismograph (OBS) profile KPR2020-2 in this study, whose circles show OBS positions, and yellow fill indicate useful data. The numbers show the OBS positions represented in Figs 3–7. Black solid lines (Kpr40, Kpr41) represent the seismic refraction profiles from Nishizawa et al. (2016).

structure of the southern KPR, this study used a 217 km long wide-angle seismic profile (ID: KPR2020-2) to estimate the structure of the crust and the uppermost mantle across the KPR near 12°N. Comparing it with the crustal structure of the above two profiles will provide key information on the growth of the KPR in this area.

2 Geological settings

Based on petrological and geomagnetic data, the tectonic evolution history of the Philippine Sea Plate has been well understood (Stern and Bloomer, 1992; Bloomer et al., 1995; Kobayashi et al., 1995; Okino et al., 1999; Hall, 2002; Stern et al., 2004). The first stage is the formation of the WPB, which is a back-arc basin developed with the seafloor spreading starting at around 55 Ma BP (Deschamps and Lallemand, 2002). Then, during 50–52 Ma BP, the Paleo-Pacific Plate began to subduct beneath the WPB, forming initial lithosphere subsidence along the eastern edge of the WPB (Ishizuka et al., 2011a). At 43 Ma BP, when the abrupt change of the Pacific Plate movement from NNW to NWW occurred, the subsidence of the lithosphere evolved into subduction (Richards and Lithgow-Bertelloni, 1996), indicating that the initial subduction lasted about 7 Ma (Ishizuka et al., 2011a). The International Ocean Discovery Program (IODP) has successively carried out two expeditions in this area (IODP Expeditions 351 and 352). Their results indicated that the fore-arc seafloor spreading occurred before the initiation of the subduction, then with the continuous subduction of the proto-Pacific Plate, the proto-IBM arc was formed within the fore-arc oceanic basin (Arculus et al., 2015; Reagan et al., 2017; Ishizuka et al., 2018). Based on the age and geochemical characteristics of the dredged samples along the entire KPR, Ishizuka et al. (2011b) concluded that the activity timing of KPR is 25–48 Ma BP, but most ages of the dredged samples fall into a narrow range of 25–28 Ma BP. The proto-IBM arc is dominated by island arc porphyry and calc-alkaline basalt (Ishizuka et al., 2018). After the formation of the proto-IBM arc, rifting and seafloor spreading occurred in the proto-IBM arc at about 30 Ma BP, forming the Shikoku Sea Basin (30–15 Ma BP; Okino et al., 1994) and the PVB (29–12 Ma BP; Okino et al., 1999) between the residual KPR and the present IBM arc (Fig. 1). These two spreading systems connected at 20 Ma BP and ceased spreading around 15 Ma BP. The spreading center jumped eastward with the retreat of the Pacific Plate, which opened the Mariana Trough at 3–4 Ma BP (Stern et al., 2004).

3 Ocean bottom seismograph (OBS) data

3.1 *Data acquisition and processing*

The seismic source was a 4×32.7 L air-gun array shot at an av-

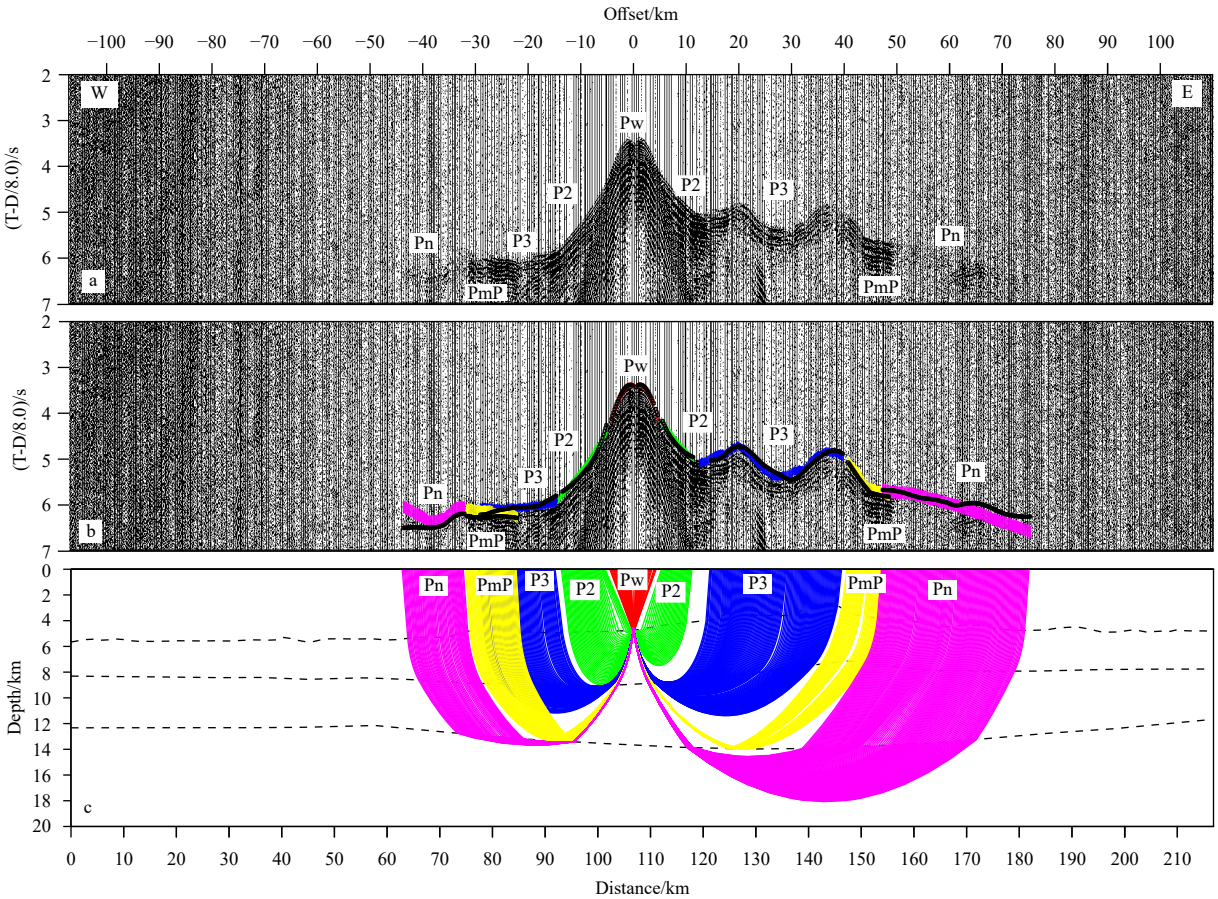

Fig. 3. An original seismic record section of the vertical component of OBS7 (a), the record section with picked and calculated travel time overlain (b), and a simulation of ray-tracing (c). T-D represents vertical component data of OBS. In these diagrams, the reduction velocity is 8.0 km/s. The names of phases are explained in the text. In b, black dots represent the predicted travel time, and the colored vertical bars represent the observed travel time in the same color of rays in c. The size of the vertical bars indicates twice the uncertainty (Zelt and Smith, 1992). In c, the colored lines represent the ray paths of different phases. The black dashed lines represent the seabed, the interface between oceanic Layer 2 and Layer 3, and the Moho discontinuity respectively, from top to bottom.

erage shooting interval of 200 m with a pressure of 10.79 MPa every 78–97 s. Here, this study focuses on the 217 km seismic profile KPR2020-2 with 1 083 shots (red line in Fig. 2). The OBS is composed of 4.5 Hz four-component geophones. Ten OBSs recorded good data sets, whereas OBS1 and OBS2 in the west and OBS13 in the east failed (Fig. 2). This study determined P wave velocities using the hydrophone component. For OBS5, the vertical component was used, as poor signals were recorded in its hydrophone component. The processing of OBS data included correction for OBS clock drift, relocation of OBSs and shots using direct arrivals, and bandpass filtering at 4–20 Hz. A final straight-line approximation of the profile was determined by least squares fit to all the shots on the profile. The depth of each OBS was first roughly determined from multi-beam bathymetric data, and then refined by fitting direct arrivals.

3.2 *Phase analysis and selection*

In general, the seismic data quality is good. Phases are identified using initial travel time modeling. This study identified the direct water wave labeled Pw, the refracted wave from oceanic Layer 2 labeled P2, the refracted wave from oceanic Layer 3 labeled P3, the Moho reflection labeled PmP, and the refracted wave from the upper mantle labeled Pn.

Clear Pw, P2, P3, PmP and Pn phases were observed at most OBSs, especially OBSs5–11 deployed above the KPR (Figs 3–7). A maximum offset of the Pn phase was observed up to 85 km, which made a good overlap control for the model. Travel-time uncertainties were dominated by picking uncertainties, which were estimated as 50 ms, 60 ms, 80 ms, 100 ms and 120 ms for Pw, P2, P3, PmP and Pn arrivals, respectively.

OBS7 was deployed at the western part of the KPR. Clearly, P2, P3, PmP and Pn phases were observed at both sides of OBS7, PmP phase was found at offsets about 20 km and 40 km of its western and eastern sides, respectively (Fig. 3). OBS8 was deployed 15 km east of OBS7. Clearly, P2, P3, PmP and Pn phases were found at its both sides, and PmP phase was found at offsets starting at 20 km and 33 km of its western and eastern sides, respectively (Fig. 4). OBS9 was deployed at the center of the KPR, 15 km east of OBS8, and P2, P3, and Pn phases were also found at both its sides, but PmP phase was found only at offsets starting at 35 km of its eastern side (Fig. 5). OBS10 was deployed at 15 km east of OBS9. Clearly, PmP phase was observed at offsets of 30 km and 15 km at its western and eastern sides, respectively (Fig. 6). Although PmP phase was found only at the western side of OBS11 with an offset starting at about 30 km (Fig. 7), P2, P3, and Pn phases were observed clearly at OBS10 and OBS11. A few arrivals may not be fitted well, which may be due to the rugged topography across the KPR.

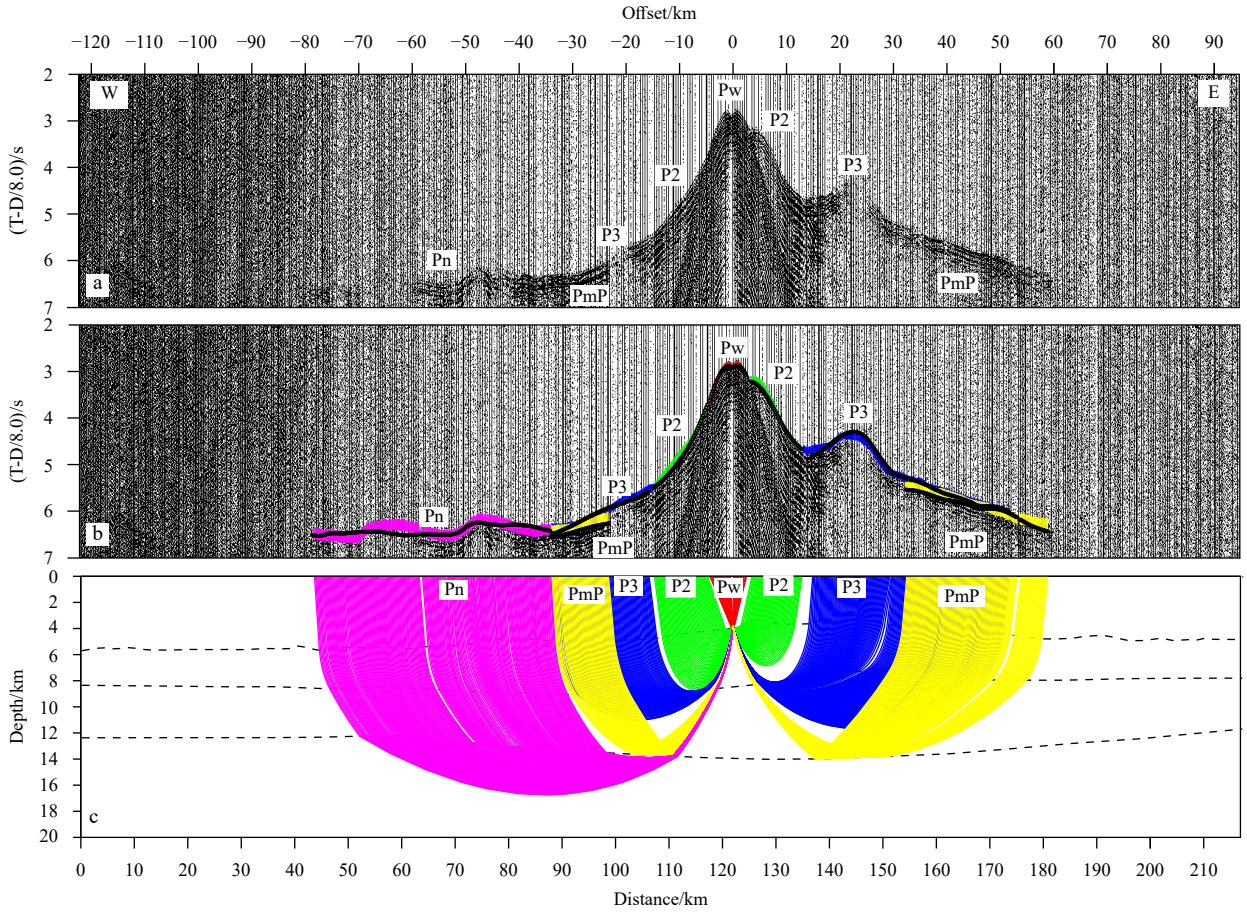

Fig. 4. An original seismic record section of the vertical component of OBS8 (a), the record section with picked and calculated travel time overlain (b), and a simulation of ray-tracing (c). T-D represents vertical component data of OBS. In these diagrams, the reduction velocity is 8.0 km/s. The names of phases are explained in the text. In b, black dots represent the predicted travel time, and the colored vertical bars represent the observed travel time in the same color of rays in c. The size of the vertical bars indicates twice the uncertainty (Zelt and Smith, 1992). In c, the colored lines represent the ray paths of different phases. The black dashed lines represent the seabed, the interface between oceanic Layer 2 and Layer 3, and the Moho discontinuity respectively, from top to bottom.

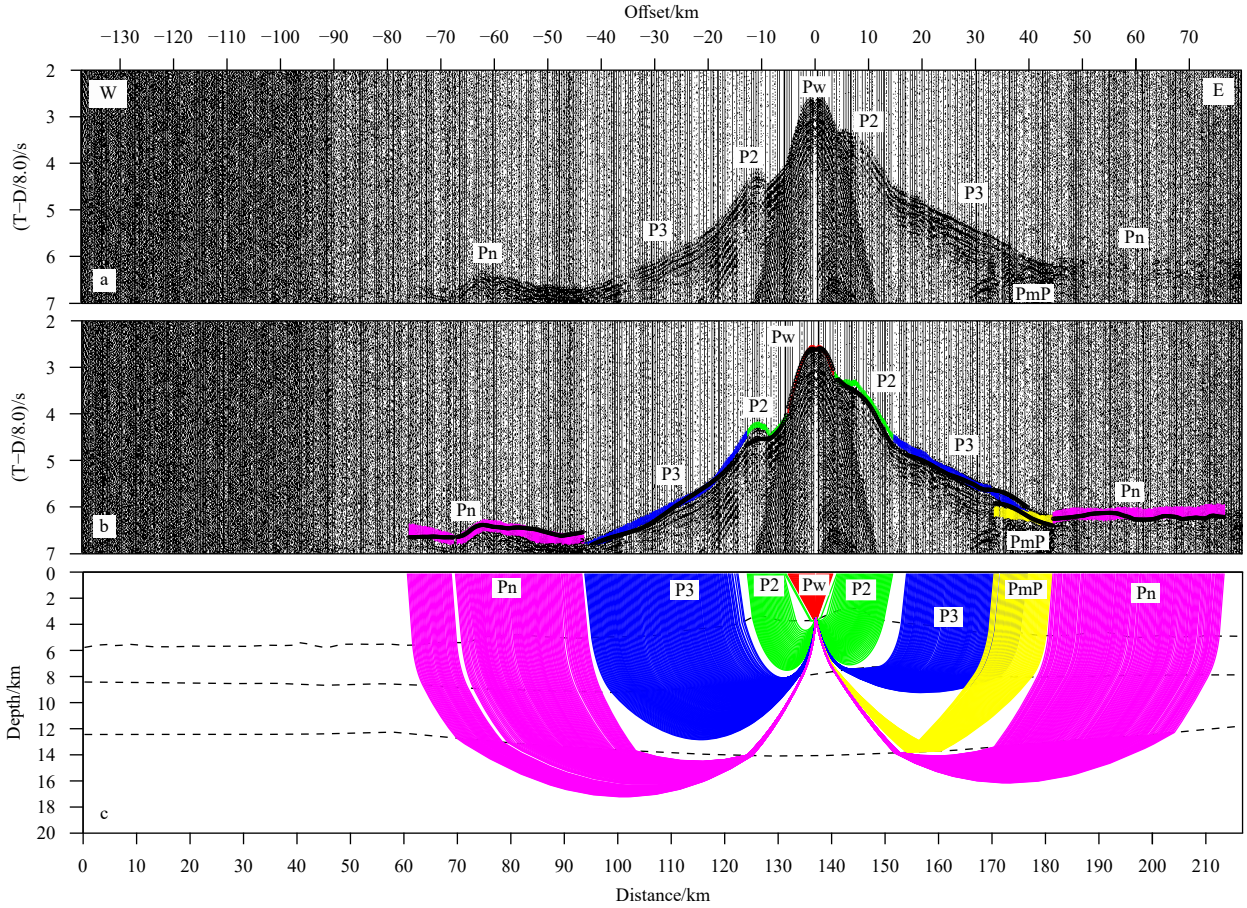

Fig. 5. An original seismic record section of the vertical component of OBS9 (a), the record section with picked and calculated travel time overlain (b), and a simulation of ray-tracing (c). T-D represents vertical component data of OBS. In these diagrams, the reduction velocity is 8.0 km/s. The names of phases are explained in the text. In b, black dots represent the predicted travel time, and the colored vertical bars represent the observed travel time in the same color of rays in c. The size of the vertical bars indicates twice the uncertainty (Zelt and Smith, 1992). In c, the colored lines represent the ray paths of different phases. The black dashed lines represent the seabed, the interface between oceanic Layer 2 and Layer 3, and the Moho discontinuity respectively, from top to bottom.

3.3 *Modeling method*

Travel time modelling and inversion approach of Zelt and Smith (1992) were used to construct velocity models. The initial model consisted of two crustal layers, representing oceanic layers 2 and 3, with linear gradients within these layers and no velocity discontinuity between them. Oceanic Layer 2 was 2 km thick and had velocities of 1.8 km/s at the top and 6.4 km/s at the bottom, whereas oceanic Layer 3 was 4 km thick and had velocities of 6.4 km/s at the top and 7.0 km/s at the bottom. The upper mantle had a velocity of 8.0 km/s at the top. The horizontal node spacings within oceanic Layers 2 and 3 were 5 km. In the upper mantle, the node spacing was 50 km. This model was based on global averages of the oceanic crustal structure (Kennett, 1982; White et al., 1992). As described by Zelt and Smith (1992), velocities and boundaries were initially adjusted manually by trial and error. After this forward modeling, a damped least squares inversion was conducted to optimize the velocity within each layer, while keeping the layer boundaries fixed.

4 Velocity results

4.1 *Velocity structures*

Along the profile KPR2020-2, the average thicknesses of oceanic crust Layer 2 and oceanic crust Layer 3 were ~3.5 km and 4.7 km, respectively, and the average velocities in Layer 2 and Layer 3 were 4.2 km/s and 6.7 km/s, respectively. As a result, the vertical velocity gradient within Layer 2 was high (average is 1.2 s^{-1}), while within Layer 3 was low (average is 0.2 s^{-1}). The velocity at the top of the upper mantle was 7.8 km/s. According to the tomography features and internal structures, this study divided the seismic profile into three parts: WPB (0–70 km), KPR (70–170 km), PVB (170–217 km).

Beneath the WPB, Layers 2 and 3 had roughly constant thickness (2.7 km and 3.8 km, respectively), and different vertical velocity gradients (~1.6 s^{-1} and ~0.2 s^{-1}, respectively). In general, lower crustal velocity of 7.0 km/s was observed at the eastern margin (60–70 km) of the WPB with few high-velocity lower crustal layers (7.3 km/s) (Fig. 8a). The Moho lies at ~12.2 km below sea level, resulting in a crustal thickness of 6.5 km. Part of the Moho reflector was controlled well by PmP (Fig. 8a).

Beneath the major part of the KPR, both crustal thickness and velocity show lateral heterogeneous. Thickness of Layer 2 changed little (between 3.7 km and 4.2 km), although the seafloor depth changed a lot (from 2.5 km to 5.0 km). The thickness of Layer 3 varied from 4.0 km at the edges of the KPR to 6.7 km in the center. Velocity varied at the top of Layer 2 (seafloor, from

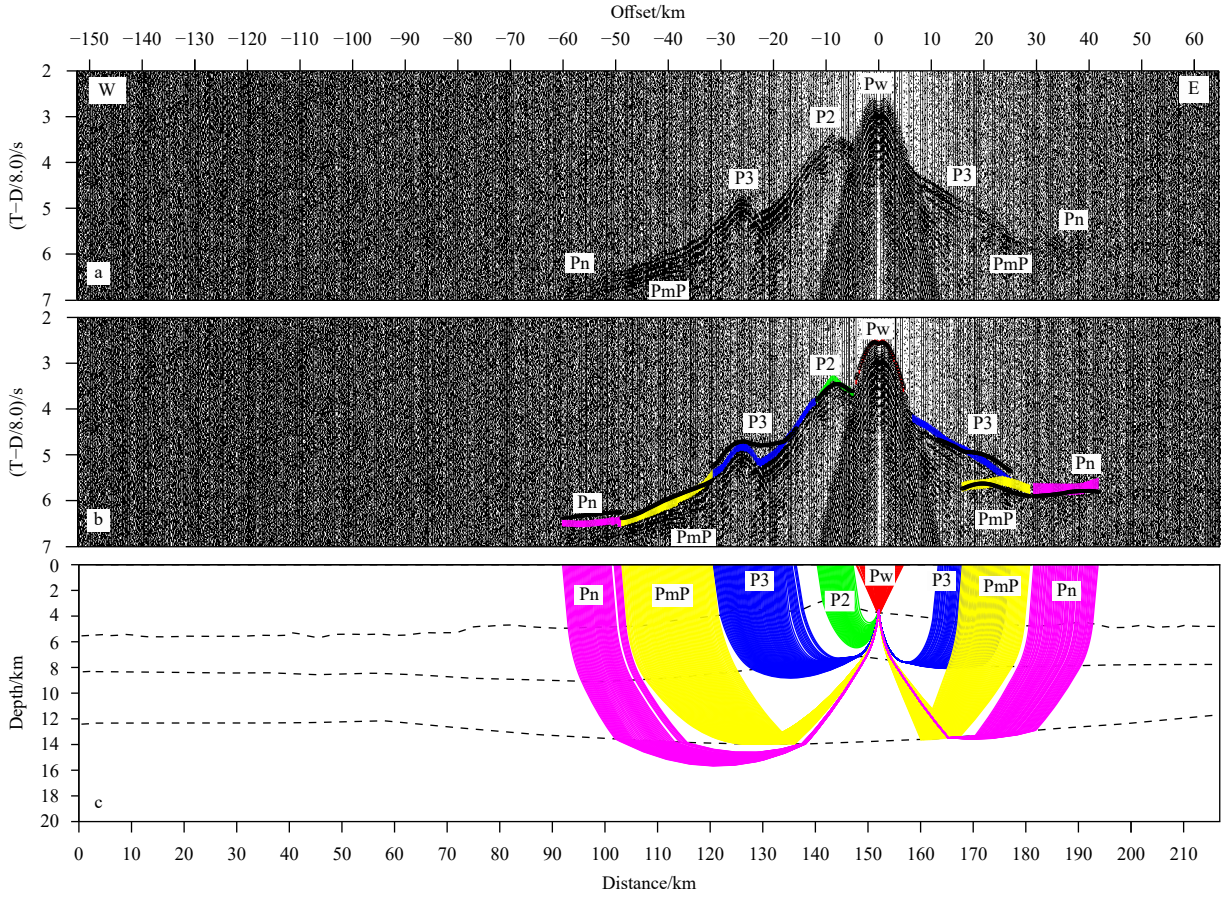

Fig. 6. An original seismic record section of the vertical component of OBS10 (a), the record section with picked and calculated travel time overlain (b), and a simulation of ray-tracing (c). T-D represents vertical component data of OBS. In these diagrams, the reduction velocity is 8.0 km/s. The names of phases are explained in the text. In b, black dots represent the predicted travel time, and the colored vertical bars represent the observed travel time in the same color of rays in c. The size of the vertical bars indicates twice the uncertainty (Zelt and Smith, 1992). In c, the colored lines represent the ray paths of different phases. The black dashed lines represent the seabed, the interface between oceanic Layer 2 and Layer 3, and the Moho discontinuity respectively, from top to bottom.

1.6 km/s to 3.2 km/s) and at the bottom of Layer 3 (6.7 km/s to 7.2 km/s), and the velocity between Layers 2 and 3 showed no discontinuities at 6.1 km/s, which is lower than that beneath the WPB and PVB (6.4 km/s). The depth of the Moho reflector was well controlled by PmP (Fig. 8a), which varied from 12.7 km to 14.0 km below sea level, sketching a relatively thicker crust ranging from to 8.2 km to 11.3 km.

The crustal structure beneath the PVB was found to be similar to that of the WPB, both Layers 2 and 3 have roughly constant thickness (3.0 km and 4.4 km, respectively), but different vertical velocity gradients (~1.5 s^{-1} and ~0.2 s^{-1}, respectively). The average V_p of the lower crust along the western margin of the PVB was less than 7 km/s. The main difference between the PVB and the WPB was the thickness of Layer 3, the Layer 3 was ~0.6 km thicker in the PVB.

4.2 *Error analysis and uncertainty*

Pick uncertainties and the travel-time misfit of the best model are provided in Table 1. The overall root-mean-square (RMS) misfit was 113 ms, and the misfit increased slightly with depth and offset. The overall χ^2 value was 1.443, with 95.0% of picks fitted, and the normalized travel time misfit suggested that the model was suitably parameterized, with a travel-time misfit a slightly bigger than the pick uncertainty. The numbers of rays through each cell were generally larger than 10 and reached over 100 (Fig. 8b), indicating that the model was well constrained. By using a perturbation test (Zelt and Smith, 1992; Muller et al., 1997), the uncertainty of the Moho depth was found to be ±0.3 km.

5 Gravity modeling and isostatic analysis

Two-dimension (2D) gravity modeling and isostatic analysis can give further constraints on the crustal model. The forward gravity response of the 2D gravity modeling is based on the 2D algorithm by Talwani et al. (1959). The free-air gravity anomaly is derived from Sandwell et al. (2014), which is a global 1′ × 1′ gravity grid. The crustal and upper mantle density model was made from the P wave velocity model in this study, where the densities for each polygon were derived from RAYINVR using its internal velocity to density conversion (Zelt and Smith, 1992). The result showed a reasonable agreement between the calculated and observed gravity anomalies along the WPB and PVB, whereas the calculated gravity under the KPR was higher than the observed (20–40 mGal, 1 Gal=1 cm/s^2) (Fig. 9). This difference might be due to the low resolution of the long-wavelength satellite derived gravity anomalies. However, the overall trend of the calculated gravity filed fits well with the observed trend, which makes good constraints on the crustal structure of the seismic refraction profile.

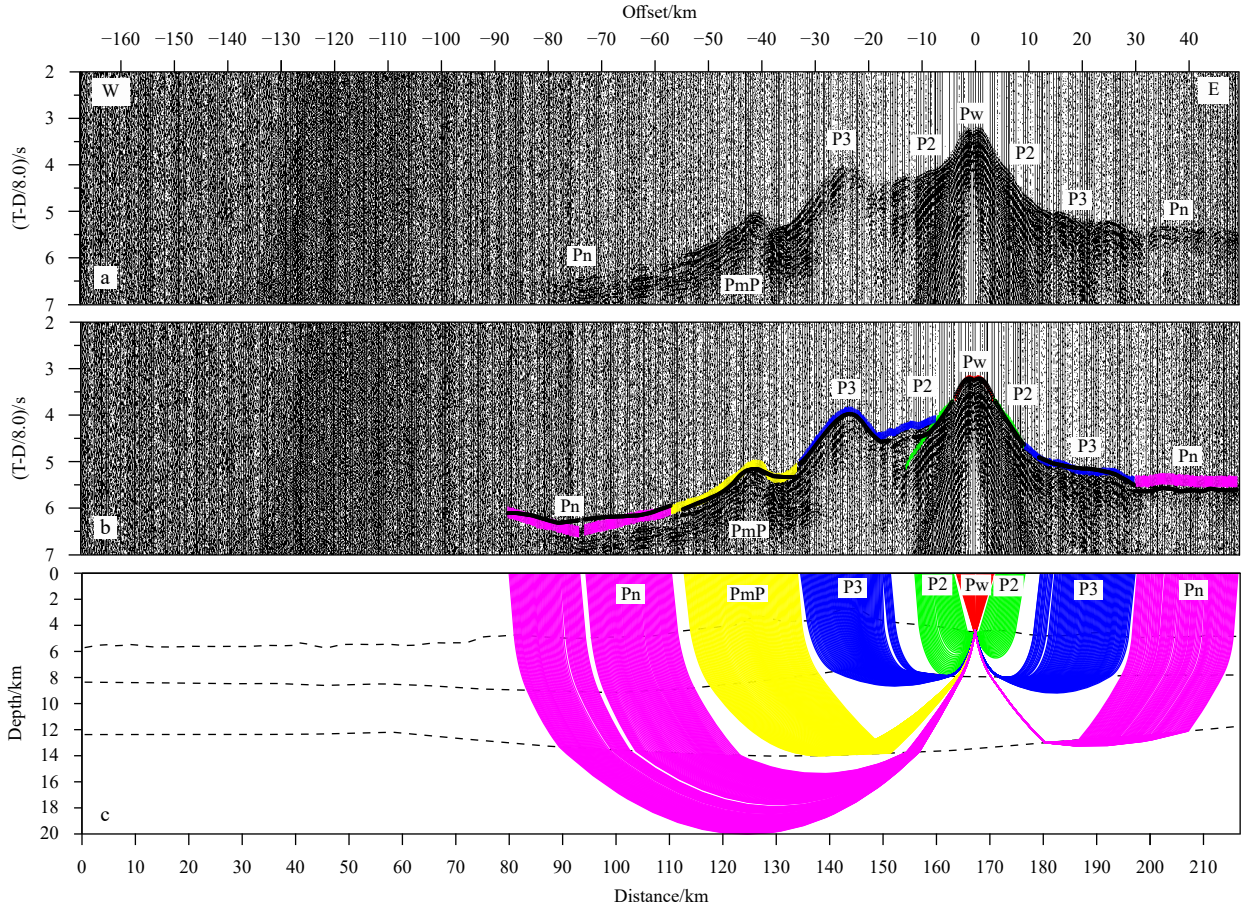

Fig. 7. An original seismic record section of the vertical component of OBS11 (a), the record section with picked and calculated travel time overlain (b), and a simulation of ray-tracing (c). T-D represents vertical component data of OBS. In these diagrams, the reduction velocity is 8.0 km/s. The names of phases are explained in the text. In b, black dots represent the predicted travel time, and the colored vertical bars represent the observed travel time in the same color of rays in c. The size of the vertical bars indicates twice the uncertainty (Zelt and Smith, 1992). In c, the colored lines represent the ray paths of different phases. The black dashed lines represent the seabed, the interface between oceanic Layer 2 and Layer 3, and the Moho discontinuity respectively, from top to bottom.

For isostatic analysis, this study calculated the pressure based on the crustal and upper mantle density model down to depth of 20 km (Fig. 9). The pressures along the WPB and PVB were 0.485 GPa and 0.495 GPa, respectively. There was no regional trend along both WPB and PVB. The difference between these two is probably due to the different oceanic lithospheric densities caused by the different ages of oceanic crust there. The pressure under the ridge was 0.51–0.52 GPa, 5.1% higher, suggesting that the KPR grew on oceanic lithosphere with some flexural strength.

6 Discussion

Early studies have shown that the velocity structure of the mature intra-oceanic island arc crust is quite different from that of submarine volcanoes that grow on the oceanic crust. The main difference is that the island arc has a thicker middle crust larger than 5 km (6.0–6.5 km/s) (Holbrook et al., 1999; Takahashi et al., 2008). The growth of the island arc results mainly from the accretion of both the middle and lower crust. The first stage includes the successive basaltic underplating caused by the partial melting of the underneath subduction plate. The second stage involves the formation of the middle crust, which comes from the initial basaltic crust differentiating to generate a crust with intermediate to felsic components with higher SiO_2 content (Takahashi et al., 2007, 2008).

Previous studies show that the development of the southern KPR has two stages (Stern et al., 2004). The first stage includes early initial island arc formation caused by the subduction of the paleo-Pacific Plate under the WPB starting at 45 Ma BP (Ishizuka et al., 2011a), forming the proto-IBM arc. The second stage involves the splitting of the proto-IBM arc and back-arc seafloor spreading of the PVB between 30–28 Ma BP (Stern et al., 2004; Okino et al., 1994; Ishizuka et al., 2011a; Grevemeyer et al., 2021), producing the relic KPR and the present IBM island arc. If the KPR is composed of the initial island arc, the crustal structure should resemble a velocity structure of the mature arc island. However, if the growth of the KPR is dominated by the magmatism related to the later stage back-arc spreading, the original velocity structure of the KPR could be modified, which could be similar to the structure of typical oceanic submarine volcanoes.

Based on the seismic velocity model, the KPR crust of this study can be divided into the upper crust (<6.4 m/s), and lower crust (6.4–7.2 km/s). The crustal thickness of the KPR is up to 12 km, but it gradually decreases to 5–6 km on both sides adjoining the WPB and PVB. The crustal structures of the WPB and PVB are consistent with results obtained from earlier seismic studies

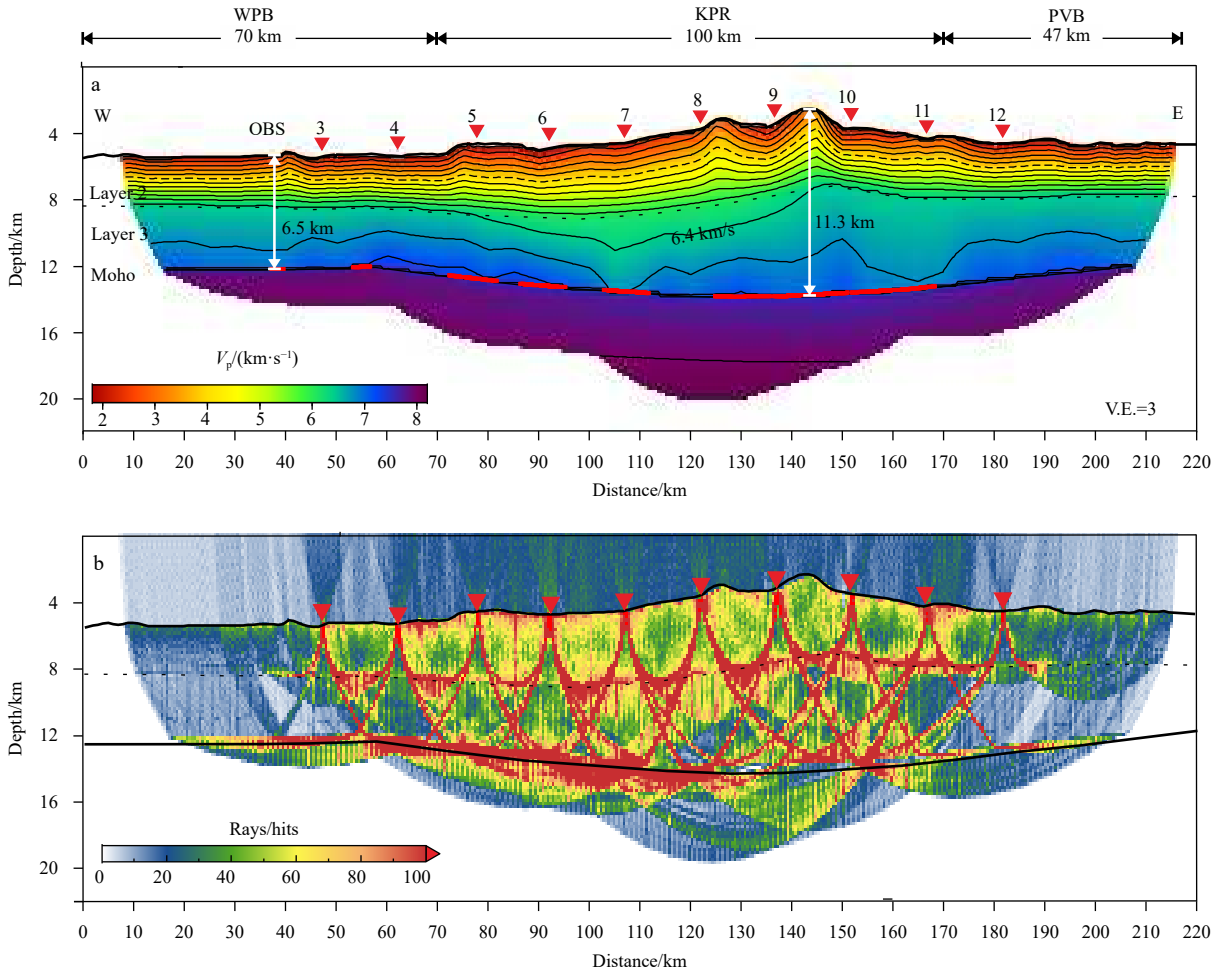

Fig. 8. The final velocity model along the profile (a) and the distribution of the ray density along the profile (b), the size of the statistic network is 0.5 km×0.2 km. Numbered red triangles represent the OBS stations. Thin black lines represent the velocity contours every 0.4 km/s. Thick black lines represent the seabed and the Moho discontinuity. On the Moho discontinuity, the red colored portions indicate sections constrained the PmP reflections. The thin dotted black line represents the interface between oceanic Layers 2 and 3. The thin dashed line represents P wave velocity contour of 4.0 km/s. The white lines with notes mark the crust thicknesses.

Table 1. Statistics of travel-time analysis

Phase	Total picks	Inverted picks	Fit ratio/%	RMS/ms	χ^2
Pw	456	447	98.0	36	0.521
P2	604	543	89.9	101	2.813
P3	2 100	1 929	91.9	98	1.528
PmP	1 069	1 053	98.5	90	0.913
Pn	2 126	2 124	99.9	146	1.476
All	6 416	6 094	95.0	113	1.443

Note: RMS, root-mean-square.

in this area (Arisaka et al., 2003; Nishizawa et al., 2007, 2016). The crustal velocity structure under the KPR is comparable to the profile Kpr41, but shows remarkable difference with that of the profile Kpr40. The latter has a thick (>5 km) middle crustal layer with a thick (~5 km) high-velocity lower crustal layer of 7.2 km/s. (Nishizawa et al., 2016) (Fig. 2). Compared to the Atlantic Ocean 0–127 Ma oceanic crustal structures, the velocity structure under the KPR is similar to that of the oceanic crust (White et al., 1992) (Fig. 10). The thick middle crust (>5 km) that observed in the mature intra-oceanic island arc crust was not observed in the velocity model of this study, which indicates that the KPR in the study area has immature island arc nature.

Back-arc spreading usually accompanies arc development (Martinez and Taylor, 2002; Dunn and Martinez, 2011). Consequently, magmatism during the arc splitting process could be controlled by pressure-release partial melting of fertile mantle. The crustal structure formed by this process is similar to the velocity structure of normal oceanic crust.

The subducting slabs could also generate arc magmatism affecting KPR crustal accretion during the breakup of the arc island. In this case, it will form a thick high-velocity lower crustal layer (7.2–7.6 km/s) along the western margin of the PVB, which mainly has mafic-to-ultramafic crustal composition underplated the lower crustal layer (Eason and Dunn, 2015). However, the seismic velocity structure shows that the average V_p of the lower crust along the western margin of the PVB is less than 7 km/s. In addition, the crustal thickness changes gradually from the KPR to the PVB, indicating that the rifting of the KPR is accompanied by a large amount of magmatism. Thus, this study suggest that the absence of the middle crust and thick high-velocity lower crustal layers in the southern KPR might due to the limited domination of arc magmatism, and/or the modification by the later stage magmatism related with arc rifting.

The main formation stage of the KPR can be estimated by the

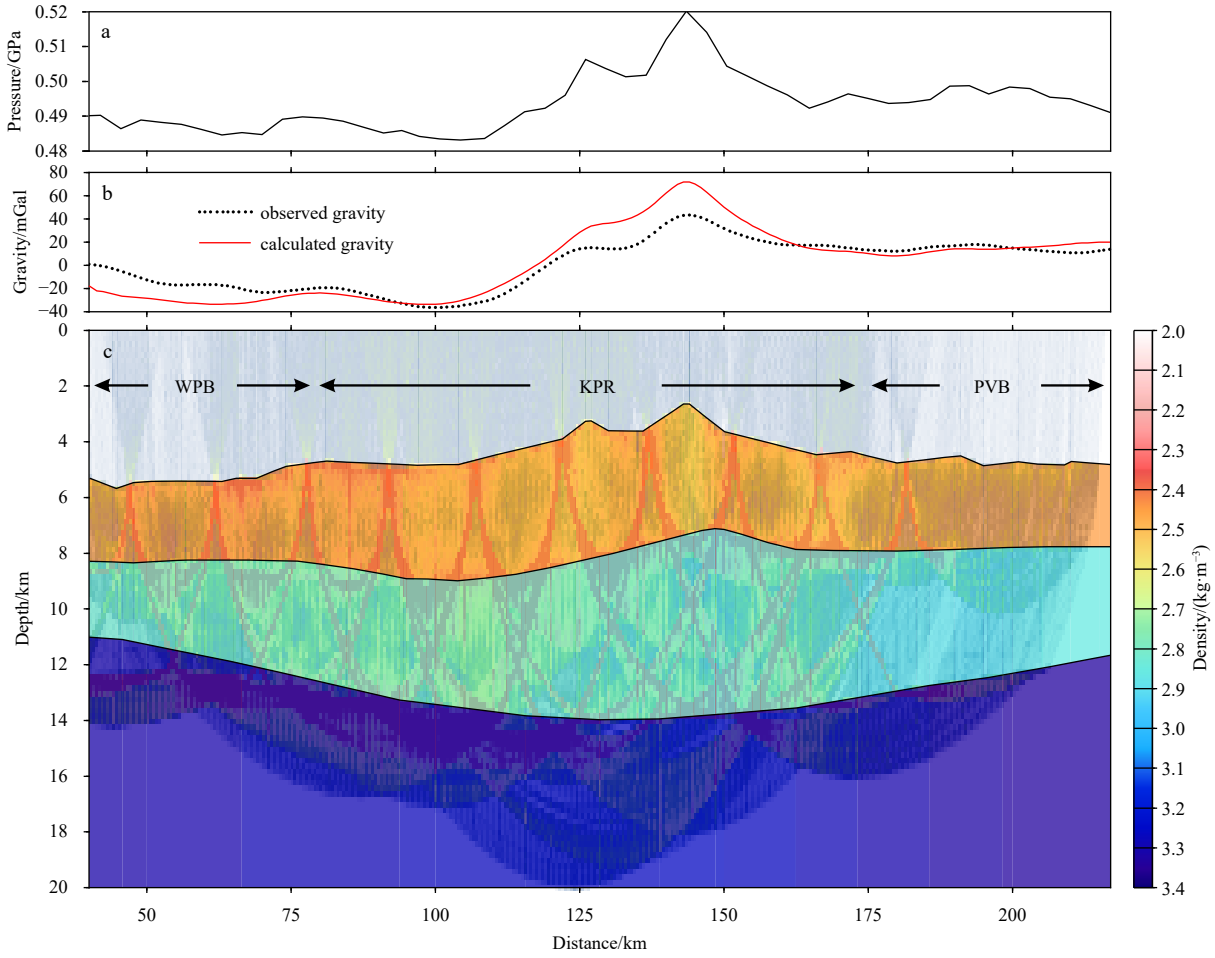

Fig. 9. Results of 2D gravity modeling of the profile KPR2020-2 from 40 km to 217 km. a. The pressure is calculated at the bottom of the model at 20 km depth; b. the results of the calculated gravity (red solid line) and observed gravity from Sandwell et al. (2014) (black dots); c. the crustal density model derived from the crustal velocity modeling. The ray density along the profile (Fig. 8b) is added as background picture in c.

plate strength at the time of the KPR loading. The IODP results show that the initial stage of the KPR formation is built by the arc magmatism (~45 Ma BP), which grew on the oceanic basin created by the fore-arc seafloor spreading starting at 50–52 Ma BP (Arculus et al., 2015; Reagan et al., 2017; Ishizuka et al., 2018). If most of the crust accretion of the KPR comes from this process, then the KPR should be formed on an oceanic plate (oceanic age 5–7 Ma) with low lithospheric plate strength. In this case, the crust should have a mountain root with nearly local isostasy compensation. At around 30 Ma BP, the rejuvenate of the KPR grew on an oceanic plate with age older than 20 Ma. If that so, the crustal structure should have some regional compensation as the ridge grew on an oceanic plate with some flexural strength. The crustal model of this study showed that the pressure under the KPR was 0.51–0.52 GPa, which is 5.1% higher than the adjacent PVB and WPB. This implies that there is some regional compensation during the loading of the KPR. Thus, this study exclude the effects of initial arc magmatism during the formation of the KPR.

In conclusion, the seismic crustal velocity structure shows that the velocity structure of KPR is more similar to an oceanic crust rather than a mature island arc. The estimation of the plate strength during the KPR loading suggests that the KPR is built mainly by the magmatism during the rifting of the proto-IBM arc between 30–28 Ma BP. The absence of the middle crust layer, larger than 5 km (6.0–6.5 km/s) and high velocity lower crustal layers (7.2–7.6 km/s) indicate that the arc magmatism plays a less important role in the KPR formation.

7 Conclusion

Travel-time modeling of active-source wide-angle seismic P wave data from OBSs deployed crossing the WPB, KPR, and PVB led to the following conclusions:

(1) This study show a high resolution crustal V_p structures beneath the WPB, KPR, and PVB. Beneath the KPR, V_p in crustal Layers 1–2, and crustal Layer 3 are 1.6–6.1 km/s and 6.1–7.2 km/s, respectively. The crustal thickness of the KPR is up to 12 km, but gradually decreases to 5–6 km on both sides adjoining the WPB and PVB. Similar crustal structures are also observed beneath the adjacent WPB in the west and PVB in the east. Only a little lateral velocity heterogeneity of less than 0.3 km/s is seen in the crust. 2D gravity modeling shows that the overall trend of the calculated gravity filed is reasonably well fit with the observed, which confirms the crustal structure of the seismic refraction profile.

(2) 1 D velocity tests show that the seismic velocity structure of the KPR is comparable to the Atlantic oceanic crust (0–127 Ma), which implies a typical oceanic crust beneath the KPR. Isostatic analysis shows that there is some regional compensation during the loading of the KPR, indicating that the initial arc-magmatism

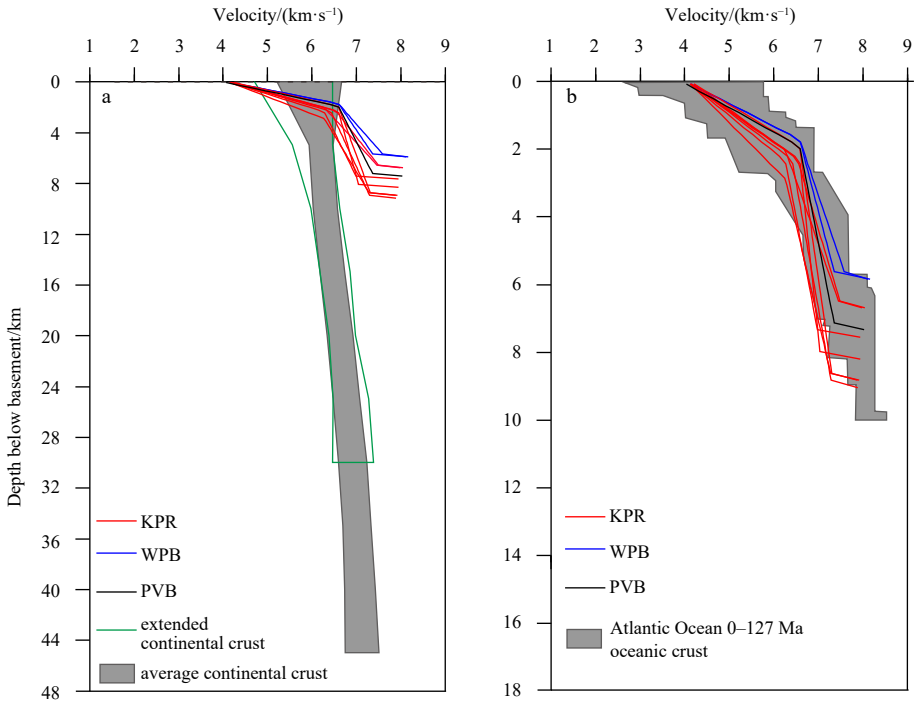

Fig. 10. A comparison of the 1D velocity curves beneath each OBS station, continental crust and Atlantic Ocean 0–127 Ma oceanic crust. In a, bold green solid line represents extended continental crust, shadow zone represents average continental crust (Christensen and Mooney, 1995). In b, shadow zone represents Atlantic Ocean 0–127 Ma oceanic crust (White et al., 1992).

is not the dominant process of the KPR formation. The absence of the thick middle crust (6.0–6.5 km/s) and thick high-velocity lower crust layer (7.2–7.6 km/s) suggest that arc-magmatism plays a less important role in the formation of the KPR.

Acknowledgements

We thank the crew of the R/V *Dayanghao*, and the technical staff and researchers involved in the West Philippine Sea 2020 Survey.

References

Arculus R J, Ishizuka O, Bogus K A, et al. 2015. A record of spontaneous subduction initiation in the Izu-Bonin-Mariana arc. Nature Geoscience, 8(9): 728–733, doi: 10.1038/ngeo2515

Arisaka M, Shinohara M, Yamada T, et al. 2003. Seismic structure of uppermost mantle and crust beneath West Philippine Basin and Kyusyu-Palau Ridge by seafloor borehole seismometer, OBS and airgun experiment. In: Proceedings of American Geophysical Union, Fall Meeting 2003. San Francisco: American Geophysical Union.

Bloomer S H, Taylor B, Macleod C J, et al. 1995. Early arc volcanism and the ophiolite problem: a perspective from drilling in the western Pacific. In: Taylor B, Natland J, eds. Active Margins and Marginal Basins of the Western Pacific, Volume 88. Washington: AGU, 67–96

Christensen N I, Mooney W D. 1995. Seismic velocity structure and composition of the continental crust: a global view. Journal of Geophysical Research: Solid Earth, 100(B6): 9761–9788, doi: 10.1029/95JB00259

Deschamps A, Lallemand S. 2002. The West Philippine Basin: an Eocene to early Oligocene back arc basin opened between two opposed subduction zones. Journal of Geophysical Research: Solid Earth, 107(B12): 2322

Dunn R A, Martinez F. 2011. Contrasting crustal production and rapid mantle transitions beneath back-arc ridges. Nature, 426(7329): 198–202

Eason D E, Dunn R A. 2015. Petrogenesis and structure of oceanic crust in the Lau back-arc basin. Earth and Planetary Science Letters, 429: 128–138, doi: 10.1016/j.epsl.2015.07.065

Grevemeyer I, Kodaira S, Guo Fujie, et al. 2021. Structure of oceanic crust in back-arc basins modulated by mantle source heterogeneity. Geology, 49(4): 468–472, doi: 10.1130/G48407.1

Hall R. 2002. Cenozoic geological and plate tectonic evolution of SE Asia and the SW Pacific: computer-based reconstructions, model and animations. Journal of Asian Earth Sciences, 20(4): 353–431, doi: 10.1016/S1367-9120(01)00069-4

Holbrook W S, Lizarralde D, McGeary S, et al. 1999. Structure and composition of the Aleutian Island arc and implications for continental crustal growth. Geology, 27(1): 31–34, doi: 10.1130/0091-7613(1999)027<0031:SACOTA>2.3.CO;2

Ishizuka O, Hickey-Vargas R, Arculus R J, et al. 2018. Age of Izu-Bonin-Mariana arc basement. Earth and Planetary Science Letters, 481: 80–90, doi: 10.1016/j.epsl.2017.10.023

Ishizuka O, Tani K, Reagan M K, et al. 2011a. The timescales of subduction initiation and subsequent evolution of an oceanic island arc. Earth and Planetary Science Letters, 306(3–4): 229–240, doi: 10.1016/j.epsl.2011.04.006

Ishizuka O, Taylor R N, Yuasa M, et al. 2011b. Making and breaking an island arc: a new perspective from the Oligocene Kyushu-Palau arc, Philippine Sea. Geochemistry, Geophysics, Geosystems, 12(5): Q05005

Kennett J. 1982. Marine Geology. Englewood Cliffs: Prentice-Hall, 813

Kobayashi K, Kasuga S, Okino K. 1995. Shikoku basin and its margins. In: Taylor B, ed. Backarc Basins: Tectonics and Magmatism. Boston: Springer, 381–405

Martinez F, Taylor B. 2002. Mantle wedge control on back-arc crustal accretion. Nature, 416(6879): 417–420, doi: 10.1038/416417a

Muller M R, Robinson C J, Minshull T A, et al. 1997. Thin crust beneath ocean drilling program borehole 735B at the Southwest Indian Ridge?. Earth and Planetary Science Letters, 148(1–2): 93–107, doi: 10.1016/S0012-821X(97)00030-7

Murauchi S, Den N, Asano S, et al. 1968. Crustal structure of the Philippine Sea. Journal of Geophysical Research, 73(10): 3143–3171, doi: 10.1029/JB073i010p03143

Nishizawa A, Kaneda K, Katagiri Y, et al. 2007. Variation in crustal structure along the Kyushu-Palau Ridge at 15–21°N on the Philippine Sea plate based on seismic refraction profiles. Earth, Planets and Space, 59(6): e17–e20

Nishizawa A, Kaneda K, Oikawa M. 2016. Crust and uppermost mantle structure of the Kyushu-Palau Ridge, remnant arc on the Philippine Sea plate. Earth, Planets and Space, 68(1): 30

Okino K, Ohara Y, Kasuga S, et al. 1999. The Philippine Sea: new survey results reveal the structure and the history of the marginal basins. Geophysical Research Letters, 26(15): 2287–2290, doi: 10.1029/1999GL900537

Okino K, Shimakawa Y, Nagaoka S. 1994. Evolution of the Shikoku basin. Journal of Geomagnetism and Geoelectricity, 46(6): 463–479, doi: 10.5636/jgg.46.463

Reagan M K, Pearce J A, Petronotis K, et al. 2017. Subduction initiation and ophiolite crust: new insights from IODP drilling. International Geology Review, 59(11): 1439–1450, doi: 10.1080/00206814.2016.1276482

Richards M A, Lithgow-Bertelloni C. 1996. Plate motion changes, the Hawaiian-Emperor Bend, and the apparent success and failure of geodynamic models. Earth and Planetary Science Letters, 137(1–4): 19–27, doi: 10.1016/0012-821X(95)00209-U

Sandwell D T, Müller R D, Smith W H F, et al. 2014. New global marine gravity model from CryoSat-2 and Jason-1 reveals buried tectonic structure. Science, 346(6205): 65–67, doi: 10.1126/science.1258213

Stern R J, Bloomer S H. 1992. Subduction zone infancy: examples from the Eocene Izu-Bonin-Mariana and Jurassic California arcs. GSA Bulletin, 104(12): 1621–1636, doi: 10.1130/0016-7606(1992)104<1621:SZIEFT>2.3.CO;2

Stern R J, Fouch M J, Klemperer S L. 2004. An overview of the Izu-Bonin-Mariana subduction factory. In: Eiler J, ed. Inside the Subduction Factory, Volume 138. Washington: American Geophysical Union, 175–222

Takahashi N, Kodaira S, Klemperer S L, et al. 2007. Crustal structure and evolution of the Mariana intra-oceanic island arc. Geology, 35(3): 203–206, doi: 10.1130/G23212A.1

Takahashi N, Kodaira S, Tatsumi Y, et al. 2008. Structure and growth of the Izu-Bonin-Mariana arc crust: 1. Seismic constraint on crust and mantle structure of the Mariana arc-back-arc system. Journal of Geophysical Research, 113(B1): B01104

Talwani M, Worzel J L, Landisman M. 1959. Rapid gravity computations for two-dimensional bodies with application to the Mendocino submarine fracture zone. Journal of Geophysical Research, 64(1): 49–59, doi: 10.1029/JZ064i001p00049

Tozer B, Sandwell D T, Smith W H F, et al. 2019. Global bathymetry and topography at 15 arc sec: SRTM15+. Earth and Space Science, 6(10): 1847–1864, doi: 10.1029/2019EA000658

White R S, McKenzie D, O'Nions R K. 1992. Oceanic crustal thickness from seismic measurements and rare earth element inversions. Journal of Geophysical Research, 97(B13): 19683–19715, doi: 10.1029/92JB01749

Zelt C A, Smith R B. 1992. Seismic traveltime inversion for 2-D crustal velocity structure. Geophysical Journal International, 108(1): 16–34, doi: 10.1111/j.1365-246X.1992.tb00836.x